Quantum gravity gradiometry for future mass change science

Ben Stray[1], Xavier Bosch-Lluis[1], Robert Thompson[1], Clayton Okino[1], Nan Yu[1], Norman Lay[1], Brian Muirhead[1], Jason Hyon[1], Holly Leopardi[2], Peter Brereton[2], Anand Mylapore[2], Bryant Loomis[2], Scott Luthcke[2], Parminder Ghuman[2], Srinivas Bettadpur[3], Maike Diana Lachmann[4], Thomas Stolz[4], Christopher Kuehl[4], Dennis Weise[4], Holger Ahlers[5], Christian Schubert[5], Ahmad Bawamia[6], Sheng-wey Chiow[1*]

[1]Jet Propulsion Laboratory, California Institute of Technology, Pasadena, 91109, CA, USA.
[2] NASA Goddard Space Flight Center, Greenbelt, 20771, MD , USA.
[3]Center for Space Research, University of Texas at Austin, Austin, 78759, TX, USA.
[4] Airbus Defence and Space GmbH, Germany.
[5] German Aerospace Center (DLR), Institute for Satellite Geodesy and Inertial Sensing, 30167, Hannover, Germany.
[6] Ferdinand-Braun-Institut gGmbH, 12489, Berlin, Germany.

*Corresponding author(s). E-mail(s): sheng-wey.chiow@jpl.nasa.gov;
Contributing authors: ben.j.stray@jpl.nasa.gov;
javier.bosch-lluis@jpl.nasa.gov; robert.j.thompson@jpl.nasa.gov;
clayton.m.okino@jpl.nasa.gov; nan.yu@jpl.nasa.gov;
norman.e.lay@jpl.nasa.gov; brian.k.muirhead@jpl.nasa.gov;
jason.j.hyon@jpl.nasa.gov; holly.f.leopardi@nasa.gov;
peter.g.brereton@nasa.gov; anand.r.mylapore@nasa.gov;
bryant.d.loomis@nasa.gov; scott.b.luthcke@nasa.gov;
p.ghuman@nasa.gov; srinivas@csr.utexas.edu;
maike_diana.lachmann@airbus.com; thomas.stolz@airbus.com;
christopher.kuehl@airbus.com; dennis.weise@airbus.com;
holger.ahlers@dlr.de; christian.schubert@dlr.de;
ahmad.bawamia@fbh-berlin.de;

Abstract

A quantum gravity gradiometer in a low Earth orbit, operating in a cross-track configuration, could be a viable single-spacecraft measurement instrument to provide mass change data for Earth observation, at comparable or better resolutions to existing maps generated by GRACE-FO. To reach the sensitivity for these science grade measurements, many parts of the cold-atom interferometer need to be operating at, or beyond, state-of-the-art performance. In order to raise the maturity of the technology of the gradiometer and determine the feasibility of a science grade instrument, a pathfinder technology demonstration platform is funded. The requirements and a notional design for such a pathfinder and the outstanding challenges for science grade instruments are presented.

Keywords: quantum sensing, gravity, geodesy, quantum gravity gradiometer, atom interferometry

1 Introduction

Measurements of the relative motion of Low Earth Orbit (LEO) spacecraft are used to estimate Earth's time variable gravitational fields, with differences used to identify mass change in all planetary domains [1]. Monitoring of lakes [2], aquifers [3], as well as ice sheets and glaciers [4], all help to study Earth's water cycle and can be used to inform wide scale resource management. Maps of Earth's gravitational field are currently delivered by the Gravity Recovery and Climate Experiment Follow-On mission (GRACE-FO) [5], which can deliver spatial resolution >150,000 km^2, at seasonal and longer (decadal) timescales, limiting the direct use for drought assessment and active resource management [6]. In order to improve the resolution of these maps, more sensitive instrumentation is required [7].

In laboratories, quantum sensors, utilizing ultra-cold atom interferometry, hold state-of-the-art sensitivities for gravity and gravity gradient measurements [8], and unlike their classical counterparts [9], have yet to reach their fundamental sensitivity limits, with active research into techniques to further improve the robustness and sensitivities of the instruments [10]. Atom interferometry is an established technique to perform absolute measurements of local gravity and, in its simplest form, is analogous to an optical Mach-Zehnder interferometer [11]: a cloud of atoms is split, mirrored, and recombined using timed laser pulses to enclose a space-time area between the two parts of the atomic wavefunction. The phase of the atom interferometer is proportional to the acceleration experienced by the atoms during the free evolution time (T) between the laser pulses along the interferometry axis. A Quantum Gravity Gradiometer (QGG) performs atom interferometry on two spatially separated cold atom samples simultaneously to get the differential gravity measurement between them, giving the scalar gravity gradient along the interferometry axis [12]. To first order, the sensitivity to gravity gradient scales as the sample separation (baseline), T^2, number of atoms, and the photon momentum exchanged during laser-atom interactions [12].

Achieving the desired measurement sensitivity to estimate time variable gravitational fields of the Earth requires a level of maturity for cold atoms that has only recently been available. Several robust systems have been demonstrated for terrestrial mapping applications [13, 14], in microgravity provided by drop towers [15–19], in parabolic flights [20], in sounding rockets [21], and operation aboard the International Space Station (ISS) [22, 23]. A Science Grade Instrument (SGI) would require beyond state-of-the-art performance in several aspects – many of which cannot be demonstrated on terrestrial platforms, requiring microgravity environments. Consequently, a pathfinder mission aims to fly a QGG instrument to demonstrate the measurement concept, qualify the design, test the performance, and determine any outstanding scientific and technical challenges required for a science-grade instrument.

2 Results

2.1 Science motivation

Regular mass change climate data records have been used to significantly advance our understanding of hydrology, oceanography, the cryosphere, and the solid Earth, becoming indispensable data for efforts to monitor and understand ongoing changes to our climate. GRACE and GRACE-FO are the second most cited NASA satellite observation in the recent IPCC 6th Assessment Report [24] and their data is a key contributor to the Global Climate Observing System (GCOS) Essential Climate Variables. Mass change data from GRACE-FO, when converted into units of radial gravity gradient, show variations of order 10 μE, where 1 E (Eötvös) is 1 nm/s^2 acceleration difference over 1 m separation (1 E = 10^{-9}/s^2).

Recognizing the scientific and societal impact of these missions, the 2017-2027 Decadal Survey for Earth Science and Applications from Space by the National Academy of Sciences identified mass change as one of five "Designated Observables," recommending that NASA both ensure continuity and seek to improve the spatial resolution relative to the program of record [25]. In response, NASA initiated the multi-center Mass Change Designated Observable study, which thoroughly analyzed a wide range of architectures and instruments that could meet the needs outlined in the Decadal Survey, with the main outcomes of the study reported in Ref. [26]. Among the architectures evaluated, a single-axis single-spacecraft QGG was found to provide better science value than a GRACE-like configuration with comparable altitude, but it was not recommended for immediate implementation as the next observing system architecture due to low technology maturity [27, 28].

The enhanced science value of the QGG relative to a GRACE-like implementation (e.g., GRACE-FO) is demonstrated in Fig. 1, which provides simulated science performance for single-axis single-spacecraft QGG for two different instrument sensitivities (standard deviations of 10 μE and 75 μE, evaluated at 10 and 20 seconds, respectively), with cross-track and radial orientations. Other errors include orbit position (1 cm standard deviation in each direction) and attitude (roll and pitch errors of 0.7 μrad standard deviation, 1.5 μrad bias, and 1.0 μrad one cycle per revolution). Angular velocity errors were not considered. Operating along the radial direction of

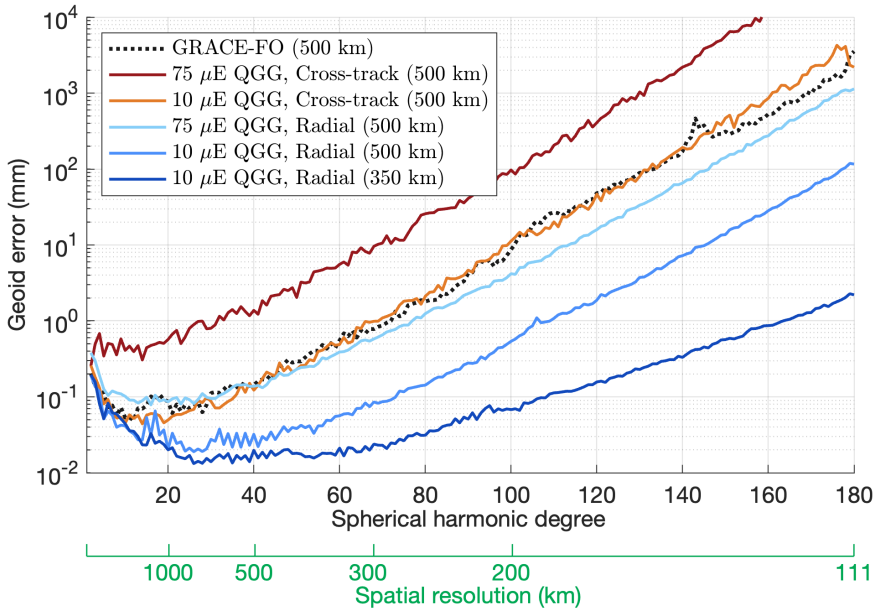


Fig. 1 Performance comparison for GRACE-FO and a single-axis QGG in different orientations, sensitivities, and orbital altitudes. Lower geoid errors at higher degrees indicate ability to measure mass change at small spatial scales.

the spacecraft yields better spatial resolution for the mass change for the same instrument sensitivity due to the projection of gravity but incurs additional engineering complexity. The radial direction rotates with the spacecraft, requiring significant rotation compensation of order mrad/s to μrad/s in LEO to yield a usable signal in the gravity gradiometer [29].

These challenges can be relaxed by operating the instrument along the cross-track direction, nominally non-rotating, which, for an instrument resolution of 10 μE, yields similar geoid error and spatial resolution as GRACE-FO but in a single spacecraft. A science-grade instrument, operating along the cross-track should therefore target sensitivities of $<$10 μE.

2.2 Pathfinder mission concept

The desired science-grade sensitivity for a quantum gravity gradiometer, requires beyond state-of-the-art performance in several areas of the atom interferometer technology [29, 30]. To provide a research platform to mature the technology in an application relevant environment, a pathfinder mission with state-of-the-art performance will be commissioned.

The objectives of the Pathfinder mission are motivated by the desired objectives of a future SGI mission. First, end-to-end system demonstration and validation of atom-interferometry-based gravity remote sensing: Long-term stability of atomic gravity gradiometry will be evaluated on the time scales from 1 minute to 90 minutes

and beyond, with instrument performance validated against known Earth gravity field measurements. Second, advances to ultracold atom interferometry technology and methods: Up to 10 s freely-falling atom interferometers will be demonstrated in microgravity, which precludes thermal-atom based instrument concepts. At the same time, the instrument should operate autonomously and continuously to demonstrate end-to-end system maturity.

The remainder of the paper describes an instrument configuration which exhibits sufficient technology maturity to meet the mission objectives in the near future.

QGG pathfinder consists of a single-axis gravity gradiometer, comprised of two spatially separated atom interferometers, measuring a differential signal in cross-track orientation of the spacecraft, aligned to the common interferometry axis. The cross-track (Y-) axis is nominally non-rotating as the craft cruises, eliminating the need for instrument rotation compensation for the QGG to operate. Operation in a near-polar orbit, similar to the orbit of GRACE-FO, will allow for potential co-fly opportunities with a future GRACE-like mission. At this orbit, the nominal cross-track gravity gradient due to Earth's gravity is 1200 E, with well-understood parts per million variations in one revolution from decades of GRACE and GRACE-FO measurement data. This available data will be used to validate the parts per hundred performance of the QGG pathfinder.

For the pathfinder mission, the gravity gradient sensitivity target along the cross-track is 100 mE/$\sqrt{Hz}$, and requiring long term stability exceeding one orbit period (>90 minutes). The instrument should also demonstrate autonomous and near-continuous operation for a sustained data-gathering period. The sensitivity objectives can be achieved with a QGG with the parameters shown in Table 1.

Table 1 Notional design parameters to reach an atom shot noise limited sensitivity of 97 mE/$\sqrt{Hz}$, calculated using Eq. (3).

Parameter	**Symbol**	**Value**
Detected number of atoms per interferometer	N_d	10^5
Effective wavevector	k_e	$8 \cdot 2\pi/780$ nm
Effective ensemble temperature	$\mathcal{T}$	100 pK
Interferometer evolution time	$2T$	10 s
Interferometer contrast	C	50%
Gradiometer baseline	L	0.3 m
Total duty cycle		14 s

Atom interferometry with ultra-cold atomic ensembles is a comparably young technology for space applications. Critical developments for its maturity towards space missions have been made in projects working with free-falling devices. In the DLR-funded QUANTUS collaboration (Quantum gases in microgravity) [31], Bose-Einstein condensates (BEC), atom interferometry, and matter-wave lensing were demonstrated for the first time in microgravity at the drop tower facility at ZARM (Bremen, Germany) [15, 16]. The step to space was taken with the MAIUS (Matter wave interferometry in microgravity) sounding rocket missions [32]. Recently, NASA's Cold Atom Laboratory (CAL) implemented atom interferometry in orbit on-board the ISS

[22, 23, 33]. The common approaches for BEC creation and technology development give crucial input to the QGG design – of specific value are the methods for fast source preparation, transport of the atomic ensembles, reduction of expansion velocities, and beam splitting processes. However, none of these platforms support high interferometer T times, limiting the demonstration of high sensitivities in a microgravity environment.

In this QGG concept, atom interferometry will be performed with multi-photon Bragg diffraction, using temporally shaped light pulses to couple momentum states of the same internal energy level. Bragg pulses have many benefits compared to more conventional two-photon Raman transitions, notably, smaller phase shift contributions from light shifts, with the remaining light shift readily compensated [34–36]. Another significant advantage of using a Bragg transition is the lesser demand on RF phase noise, thanks to a smaller optical frequency difference in Bragg transitions (few 10 kHz) than in Raman processes (few GHz) [37]. As Bragg transitions do not change the internal state, atoms can be transferred to another state and remain dark to subsequent Bragg pulses making it suitable for techniques such as interleaving interferometers. Losses due to high momentum Bragg orders are mitigated by implementation of a sequential pulse scheme that transfers $8\hbar k$ of photon momentum to the atoms.

In the following sections, we present detailed descriptions of the physics protocol and the corresponding instrument design concept. In addition to the design presented, aspects of the atomic system have been modelled to infer requirements of QGG-pathfinder presented within. Full system modelling tasks are underway and will be validated using ground-testbed results to understand the full specification and performance requirements of a science grade instrument.

3 Methods

3.1 Payload description

The target host platform should accommodate a QGG payload having Size, Weight, and Power (SWaP) parameters limited to $0.5 \times 0.5 \times 1$ m^3, 125 kg, and 350 W average power consumption, based on preliminary feasibility studies. It is desirable that the center of the QGG baseline be placed at the center of mass of the spacecraft during operation, with the interferometry axis aligned to the cross-track, and that the mass distribution of the craft be well known and modelled to reduce residual acceleration noise on the atomic systems.

The payload is split into several subsystems, consisting of: the Atomic Physics Package (APP), the Laser Optical System (LOS), the Integrated Control Electronics (ICE), and the Power Conditioning and distribution Unit (PCU), with the components and interfacing seen in Fig. 2. The APP and LOS are discussed in more detail in Sections 3.1.1 and 3.1.2, respectively.

The ICE provides the communications interface between the spacecraft and the instrument, and between instrument subsystems. It can be considered as two parts: a high-performance processor-based part for onboard processing of data and images, such as for the extraction of fringe phases and data compression, and a high-reliability Field Programmable Gate Array (FPGA) based part, used for timing control to trigger

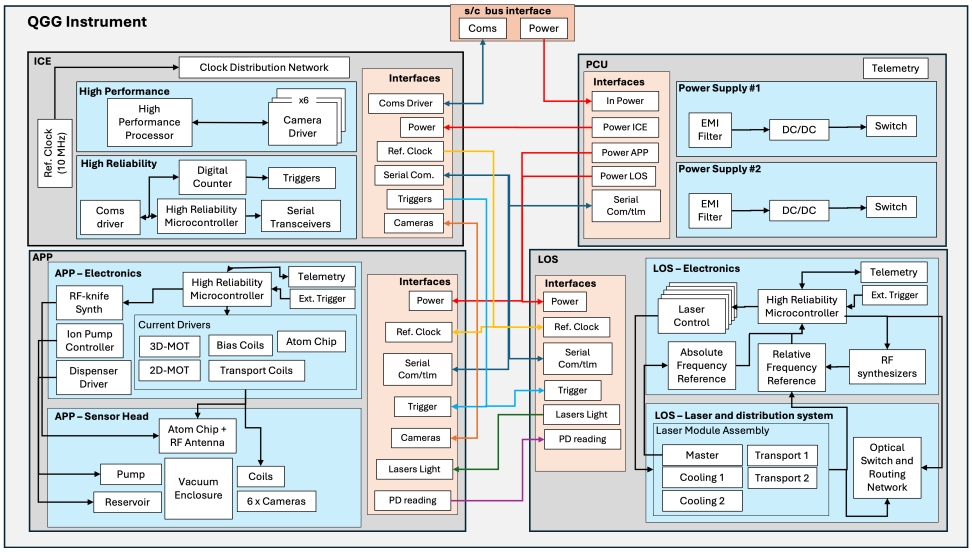


Fig. 2 Contents and interfacing between the different subsystems. QGG interacts with the spacecraft (s/c) with only communication and power.

the LOS and APP, realizing the cold atom and interferometry sequences. Configuration parameters and sequences for the modes of instrument operation are received and set by the ICE, with experimental and telemetry data sent to ground using the spacecraft communication capabilities. The sequence and timing steps can be updated from the ground for experimentation, debugging, or optimization of the instrument performance. Received sequence steps are separated and sent to APP and LOS microcontrollers for local execution upon triggers from the ICE. To ensure synchronization between subsystems, the ICE distributes a stable, low-phase noise 10 MHz reference clock.

The PCU is designed to be highly efficient, with low noise at the output, and takes a standard input of 28 V from the host bus. Input EMI filters are used to clean the voltage provided by the spacecraft, then DC/DC converters condition the voltage to the instrument subsystems and galvanically isolate the spacecraft and the instrument grounds. From this, the PCU provides a nominal power output of 385 W, with a 200 ms 775 W peak power to drive the strong gradient coils used to magnetically transfer the atomic cloud to the atom chip. To account for standard derating and aging effects, the PCU has been over-specified for the 350 W instrument power consumption. The output of the PCU has switches to selectively disable subsystems, and telemetry for diagnostics on voltage and current per subsystem. Power conditioning is completed at each subsystem, including the LOS, ICE, and APP electronics, where the voltage is regulated and filtered before being sent to components.

3.1.1 Atomic Physics Package

The atomic physics package consists of the sensor head, where the ultra-cold atom samples are generated; and the associated driving and control electronics. The sensor head consists of an ultra-high vacuum (UHV) system to remove collisions with background ambient gases, the atom source, sets of magnetic coils for generating magnetic traps, uniform fields and compensation of residual magnetic fields, optical and electrical delivery, cameras and photodiodes for detection of the atoms and optical power monitoring, and magnetic shielding to suppress ambient magnetic field variations. The UHV system is split into three connected regions, shown in Fig. 3, along with the atom transport axes.

Atoms are trapped and cooled within a non-magnetic UHV enclosure, starting from a vapor-loaded 2D-MOT. The atoms are pushed, via a 1 mm thru-hole, serving as a differential pumping stage to create a pressure difference of at least 1:1000, into the lower pressure 3D-MOT/BEC chamber. The atoms are loaded into a 3D-MOT and then magnetically transferred above an atom chip which is used to rapidly generate a BEC, with the sample then being delta-kick collimated to reach an effective temperature of the order 100 pK to limit cloud expansion [16, 32, 38, 39]. The collimated ensemble is optically transported to the interferometry region, and then split and transported using dual optical lattices to prepare two samples separated by a baseline of 0.3 m. The splitting is aligned with the interferometry axis, which is along the cross-track orientation to the spacecraft orbit. Atom interferometry is performed on both samples simultaneously, and each interferometer is read out through fluorescence imaging of the spatial fringe on the sample, detected on a camera for each cloud. This measurement is destructive, and a new sample must be generated again for the next measurement.

In order to support an interferometry $2T$ time of 10 s, and limiting losses due to collisions to $< 10\%$, the collision rate γ_a must be less than 0.01 s^{-1}, which sets the vacuum pressure requirement as follows. The pressure requirement comes from kinetic theory, relating the collision rate, $\gamma_a = \hat{v}/l$, to the mean free path, $l = k_B\mathcal{T}/(4\pi a_s^2 P)$, and mean speed, $\hat{v} = \sqrt{3k_B\mathcal{T}/m}$, with the temperature, $\mathcal{T}$, rubidium mass, m, Boltzmann constant, k_B, and collision cross-section, $4\pi a_s^2$. This results in the pressure expressed as

$$P = \frac{\sqrt{mk_B\mathcal{T}}}{4\sqrt{3}\pi a_s^2}\gamma_a. \tag{1}$$

The scattering length a_s between ^{87}Rb is $\sim 100a_0$ [40], which is several orders of magnitude larger than other expected gases in a properly fabricated UHV chamber [41]. Assuming an environment temperature of 30 °C, the partial pressure requirement of the interferometry region must be below 4×10^{-12} mbar for Rb, and 1×10^{-10} mbar for other gases, maintained by active ion-getter pumps and a passive non-evaporable getter pump.

3.1.2 Laser Optical System

The laser optical system supplies light to the APP at wavelengths near 780 nm suitable for cooling, trapping, internal state manipulation, transport, interferometry, and

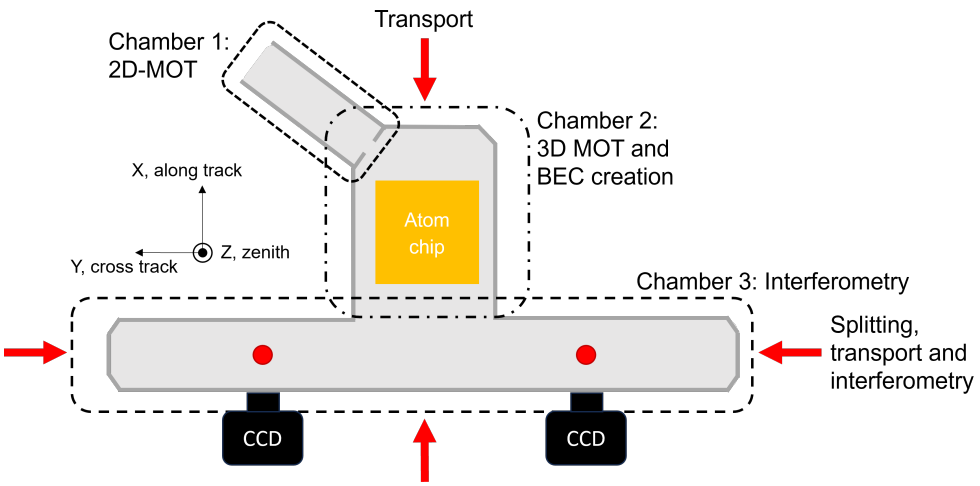


Fig. 3 Atomic physics package overview, showing a design for a single source gravity gradiometer. The three main regions are: a vapor loaded 2D-MOT, an atom chip for 3D-MOT and BEC generation, and an interferometry region. Optical transport is used to move atoms from Chamber 2 into Chamber 3 - the interferometry science region. Using an optical lattice, the single cloud is split into two and optically transported to the experiment baseline 0.3 m to create the gradiometer. Interferometry is performed in the Y-axis, cross-track to the spacecraft orbit. Atoms are imaged by CCD cameras through ports in the vacuum system. Not shown are the vacuum pumps, viewports, or laser beams for the MOT and BEC generation.

detection of ^{87}Rb atoms. During operation, light pulses at the required optical frequencies are generated and distributed to the appropriate output ports according to a configurable timing sequence.

An overview of the LOS is shown in Fig. 4. The LOS interfaces with an LOS Control system (LOSC), which is controlled by the ICE. The LOSC includes electronics required to drive the acousto- and electro-optic components inside the LOS, e.g., laser drivers and RF sources. It is also responsible for implementing the timing sequence commanded by the ICE and for performing certain tasks autonomously, such as automatic laser (re-)locking. To this end, the LOSC includes a CPU and an FPGA. A master RF reference is provided by the ICE to ensure sufficient timing accuracy and synchronisation with the APP sequence. A measurement cycle is started by an electrical trigger signal from the ICE, following which the LOSC controls each parameter according to the pre-configured timing sequence. This includes, for instance, electrical currents, RF frequencies, and switch positions.

The LOS itself includes five space-grade laser modules at 780 nm, based on a micro-integrated master-oscillator power-amplifier architecture, including external cavity diode laser (ECDL) chips and solid-state optical amplifiers (SOAs), developed as part of BECCAL [42]. Each module provides up to 350 mW of optical power in optical fiber. Laser frequency stabilisation is achieved by referencing a master laser module to a rubidium vapor cell to provide an absolute frequency reference. The master laser is locked to a ^{85}Rb transition via modulation transfer spectroscopy [43]. The other

lasers are offset phase locked to the master laser to provide light at the required frequencies determined by the offset frequency. The phase lock can be direct, or to a 1st order EOM sideband, for offset frequencies of up to 10 GHz for use with the cooling and Bragg beams, or locked to a 10th order EOM sideband to generate offset frequencies of order 100 GHz [44], for use with the optical transport beams. The frequency of each laser can thus be controlled by changing the RF frequency of a reference oscillator, providing agile frequency control of the lasers over 100s MHz. As excellent phase coherence is required between the optical transport beams, the second transport laser is injection locked to the first transport laser instead of using an offset phase lock.

Each laser module serves several functions to reduce the total number of modules required. Light from each module is sent through a series of fiber-based components, including acousto-optic modulators (AOMs) and electro-optic modulators (EOMs), before being distributed by fiber-based switches to various ports of the APP. Here, the AOMs provide fast switching and laser power control, including power stabilization to the APP via monitoring photodiodes, while the switches based on micro-electro-mechanical systems (MEMS) provide multiplexing capability and additional extinction when the light needs to be turned off. Light which needs to be in the same spatial mode but can have orthogonal polarization is efficiently superimposed using polarizing beam combiners. The repump frequency for the MOT ($|F = 1\rangle$ to $|F' = 2\rangle$) is generated from the master laser by using an EOM sideband and can be turned on and off using the driving RF signal.

High light extinction is required from the laser system between the pulses to reduce resonant photons from hitting the atoms in the free-evolution time. For the interferometer time of $2T = 10$ s, limiting losses due to leaked light to 1%, gives a photon scattering rate of 0.001 s^{-1}. Using the photon scattering rate equation for on resonant, low power atom excitation [45], the leaked light should not exceed 0.088 pW/cm^2. For the design of the laser system and APP beam parameters, the requirement for extinction is estimated as 96 dB, which can be met by the combination of AOMs and MEMS.

3.2 Physics protocol

Two Mach-Zehnder atom interferometers are operated simultaneously on two spatially separated clouds. By driving the interferometry sequences with the same light field, common mode phase noise sources are removed due to correlations in the data [46, 47]. This approach can be used to suppress many systematic errors in atom interferometers, most notably accelerations due to vibration and laser phase noise. The phase difference between two atom interferometers, to the leading order, can be expressed as

$$\phi_{QGG} = k_e \gamma L T^2, \tag{2}$$

and the atom-shot-noise-limited sensitivity of the gradiometer is given by Eq. (3), where the fractional gravity gradient, $\delta\gamma/\gamma$, is a product of the terms defined in Table 1.

$$\frac{\delta\gamma}{\gamma} = C \frac{2}{\sqrt{N_d}} \frac{1}{k_e L T^2}. \tag{3}$$

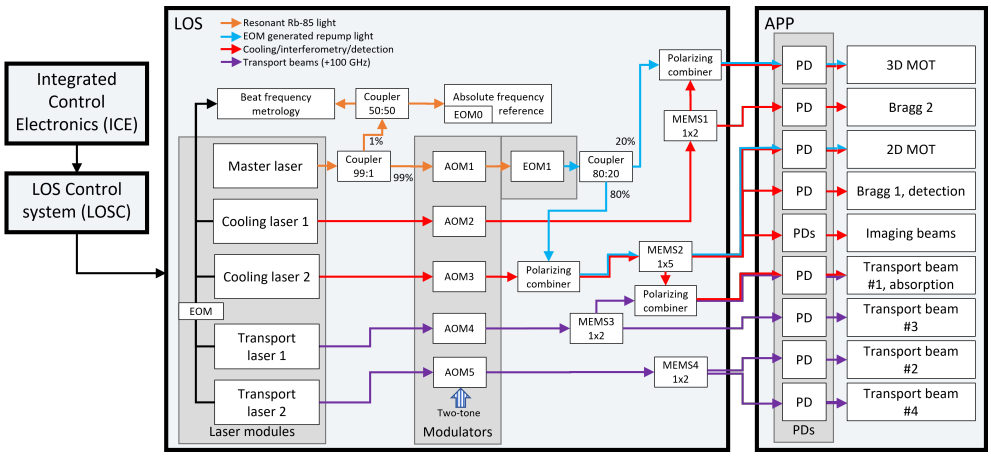


Fig. 4 LOS layout with distribution to the APP. Each laser module is offset phase locked to the master laser to enable dynamic frequency control. Polarizing combiners and MEMS switches are used to multiplex the laser light delivered to the APP. This approach reduces the total number of required laser modules by using the same laser module for different steps in the timing sequence. There are several additional EOMs and AOMs, couplers, and photodiodes (PDs), not shown that make up the beat frequency metrology module to achieve the offset phase lock for each laser.

The factor of 2 in Eq. (3) accounts for the quadrature sum of uncorrelated noise of two interferometers, and the distribution of interferometer phases in one cloud.

Since the sensitivity of the gradiometer is dependent upon the baseline between the two clouds, variations of initial cloud position reduces the sensitivity of the instrument. For the parts-per-million metrology objective of the pathfinder, this requires the initial cloud positions to be known to within few μm over the required baseline, which is difficult for two independent BEC sources. Instead, we adapt a scheme to derive each ensemble from a single source that is optically split and transported using quantized momentum and precise timing to reduce the uncertainty in baseline [16, 30].

A single measurement cycle consists of several steps that are required to prepare each interferometer's atomic ensemble before performing the interferometry sequence. The total duration of the measurement cycle is estimated to be 14 s, with 10 s of that being the $2T$ atom interferometer duration – an evolution time not achievable in terrestrial microgravity facilities.

The sequence steps and required parameters to achieve the target sensitivity of 100 mE/$\sqrt{Hz}$ are discussed in the following sections.

3.2.1 Source preparation

In each experimental cycle, two ensembles of 1.2×10^5 ultracold ^{87}Rb atoms, at equivalent temperatures of 100 pK, separated along the atom interferometry axis by 0.3 m, are required to support the long interrogation times in the interferometer. High atom number reduces the atom-shot-noise-limited sensitivity, and low temperatures reduces contrast loss due to dephasing from finite beam to cloud sizes and to fringes from

residual rotation. Generating this pair is achieved through splitting and transporting a single source BEC.

First, a 2D-MOT is generated in Chamber 1 in Fig. 3, which generates a cold atomic beam from background vapor. The atomic beam passes through the differential pumping stage and is used to load a six beam 3D-MOT in Chamber 2. Polarization gradient cooling after the 3D-MOT is performed on the atomic cloud to reduce the temperature to the μK regime, before being prepared in the magnetically sensitive state $|F = 2, m_F = 2\rangle$ by optical pumping. The sample is then magnetically trapped and transported to a magnetic trap above the in-vacuum atom chip. A BEC is generated above the surface of the atom chip from the magnetically trapped atoms by RF-forced evaporative cooling [48].

In order to further reduce the expansion velocity of the ensemble, delta-kick collimation (DKC) is performed [16, 32, 38, 39], where the ensemble is released for free expansion and after some time a magnetic potential is applied. The velocity distribution of the ensemble is manipulated resulting in a lensing effect and a low expansion velocity in the range of a temperature equivalent of 100 pK. The atoms are then prepared into the magnetically insensitive state $|F = 1, m_F = 0\rangle$ through a scheme using RF fields [22, 32, 49] and Doppler-free two-photon Raman transitions.

The atoms are loaded into an optical lattice that is accelerated to optically transport the ensemble from the atom chip region into Chamber 3 – the interferometry chamber [50, 51]. Finally, the atoms are loaded into a second optical lattice, aligned to the interferometry axis which is used to split the sample into two and accelerate the two halves in each direction. This is achieved through chirping the frequency of each lattice beam to create two lattices moving in opposite directions [52]. By adiabatically loading and unloading the lattice, efficient transport should be readily achieved. Each cloud is decelerated in the optical lattice to create the two ensembles separated by 0.3 m. Through imposing a fixed number of momenta during the optical transport and precise timing control, the separation of the two clouds should also be determinate [53], providing the required two ensembles for the gradiometer.

3.2.2 Atom interferometer

Atom interferometry is performed using multi-photon Bragg diffraction, scattering $2n$ photons from a pair of counter-propagating beams, without changing the internal state. Bragg diffraction offers a few advantages over Doppler-sensitive two-photon Raman transitions when implemented in a SWaP limited system. The requirements on the laser and RF chain are much less stringent for Bragg diffraction, requiring lower RF frequencies, and thus lower power amplifiers, than counter-propagating Raman transitions. For increasing the sensitivity of the gradiometer, it is also easier to implement large-momentum transfer using Bragg diffraction, with momentum of $> 100\hbar k$ demonstrated [51, 54]. Since the interferometry occurs within the same internal energy state $|F = 1, m_F = 0\rangle$, relying on the interference between momentum states, the population can be shelved to the upper ground state $|F = 2, m_F = 0\rangle$, allowing for more complex multiplexing schemes for interleaved operation of interferometers.

In this implementation, multi-photon Bragg transitions are used to coherently transfer atoms between momentum states $|0\hbar k\rangle$ and $|\pm 4\hbar k\rangle$, with each beam splitter

pulse consisting of several sequential light pulses. The beam splitter pulse is constructed from a $\pi/2$-pulse, which transfers half of the population from state $|0\hbar k\rangle$ to $|+4\hbar k\rangle$, followed by a π-pulse transferring the remaining atoms in $|0\hbar k\rangle$ to $|-4\hbar k\rangle$, effectively implementing a symmetrized beam splitter, as described in Ref. [55], but for Bragg instead of Raman transitions. The selective transitions are done by tuning the frequency of the counter-propagating beams to be resonant with different Bragg transitions. Sequential pulses are chosen over directly driving double-diffraction [29] to remove losses due to undesired Bragg transitions, such as $|0\hbar k\rangle$ to $|\pm 2\hbar k\rangle$ or $|\pm 6\hbar k\rangle$, which are also resonantly induced by the standing waves in the retro-reflected lattice. The mirror pulse is constructed of three π-pulses, transferring the atoms from $|+4\hbar k\rangle$ to $|0\hbar k\rangle$, then all atoms from $|0\hbar k\rangle$ to $|-4\hbar k\rangle$ and vice versa, before finally $|0\hbar k\rangle$ to $|+4\hbar k\rangle$ to reverse the momentum of both arms. The final beam splitter follows the opposite scheme to the opening beam splitter, which can all be seen in Fig. 5. The pulses have a Gaussian temporal profile, with a width of around 100 μs and variable amplitudes, where the interferometer contrast may later be improved from optimal control schemes [56]. This pulse scheme does introduce laser phase noise due to targeting only one of the interferometer arms at a time; however, when used for the gradiometer measurement, this phase noise is common to both interferometers and thus removed in the differential measurement.

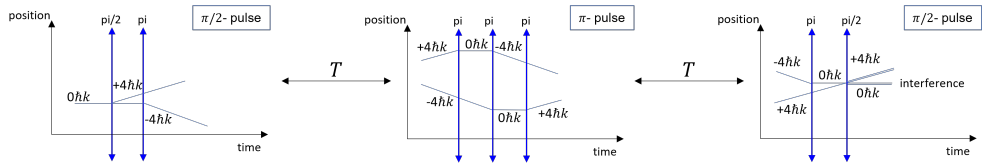


Fig. 5 Interferometry scheme utilising sequential Bragg diffraction to achieve $8\hbar k$ momentum splitting. Each beamsplitter and mirror pulse is constructed from several Bragg pulses to avoid losses due to undesired Bragg transitions. This scheme is performed on both atomic ensembles simultaneously, with the added phase noise from addressing a single arm common to each interferometer and thus removed in the differential measurement.

3.2.3 Detection

The interferometer can be read out through imaging spatial fringes on the output ensembles [57–61]. Fringes can occur due to the gravity gradient, uncompensated Coriolis forces, or be introduced by asymmetric timings to open the interferometers [57–60, 62, 63]. As both interferometers should experience the same external uniform accelerations or timing asymmetry, a deviation in their spatial fringe patterns shows a differential acceleration between both interferometers, which is caused by gravity gradients and other systematic effects, such as magnetic field inhomogeneity. Measuring the phase difference between the fringe patterns of the interferometers in each measurement cycle can yield a gravity gradient measurement in a single experimental run, in contrast to the fringe-free single-detector readout scheme.

In the pathfinder, 240 ms after the final beam splitter pulse, the output ports of the interferometers have spatially separated by few final ensemble radii, and spatial fringes have emerged. The spatial density distribution of the atoms can be imaged using fluorescence imaging, with both interferometers illuminated by the same resonant light for around 100 μs, destroying the ensembles through heating. The emitted photons are collected on a dedicated camera per interferometer. Optionally, a reference image can be taken after the ensemble is dispersed to better distinguish fluorescence photons from background scattering. Pre-processing and calculations such as interferometer phases can be performed on-board by the ICE to reduce down-link data volume.

Contrast loss of the fringes is mostly caused by phase variation across the cloud as seen in the imaging direction, where atomic population is integrated over [53, 62–64]. The main uncontrolled contributors in the QGG pathfinder configuration are residual rotation across the camera field of view (the Coriolis phase term) [57, 65], and beam pointing jitter in the camera line-of-sight [58]. For interferometer contrast of >50% and to eliminate the need for a rotation compensation system, the detection scheme requires the spacecraft to provide attitude control of better than 15 μrad over the interferometer time, orientate to the cross-track to within 1 mrad, and have residual rotation of 1 μrad/s. These requirements ensure the phase variation across the cloud is less than 1 rad in the line-of-sight of the imaging camera [53, 62–64].

4 Discussion

4.1 Error budget

The instrument sensitivity is determined by the combination of the noise sources in the measurements. For the anticipated 10^5 atoms in the interferometer and a fringe contrast of 50%, the quantum projection noise, the uncertainty of differential interferometer phase determined by the number of atoms in the interferometer, is 12.6 mrad per run, corresponding to a sensitivity of 97 mE at 1 s, from Eq. (2). For the instrument to be atom shot noise limited, with the quantum projection noise being the dominant noise source, all other contributions must be suppressed below that. The notional experimental parameters expressed in Table 1 are used in the atomic system model to determine the effect of different errors on the interferometer and gradiometer output. Major error terms have been modelled so far, and can be grouped by noise (Table 2) and systematic terms (Table 3).

4.2 Concept of operations

The QGG Pathfinder Mission consists of three mission elements. The QGG Pathfinder Space Element (SE) is the space observatory that will include the spacecraft, the QGG Pathfinder Instrument and ancillary systems. The Launch Element (LE) is the launch vehicle and corresponding support services. The LE is also expected to include all facilities and equipment needed to support integration, support, and control functions as well as ground support equipment related to the LE. The QGG Ground Element (GE) will consist of the ground systems, equipment, and personnel needed to support mission control functions and all the interfaces needed with existing ground stations

Table 2 Anticipated leading instrument noise sources and their phase noise budget for the differential atom interferometers per measurement cycle. Parameters used for evaluating the terms (in addition to those listed on Table 1): Bragg diffraction order $n = 4$, $\pi/2$-pulse duration $\tau_R = 100$ μs, speed of light c, nominal gravity gradient $\gamma = 1200$ E, nominal orbiting rate $\Omega = 1$ mrad/s.

Noise source	**Formula**	**Contribution**	**Comment**
Quantum projection noise	$2/(C\sqrt{N_d})$	12.6 mrad	Assuming uncorrelated noise between interferometers.
Laser frequency noise, S_ν^0	$2\pi^2 n \frac{L}{c}\sqrt{\frac{S_\nu^0}{\tau_R}}$	2 mrad	Assuming white frequency noise of Bragg laser $S_\nu^0 = 64 \times 10^3$ Hz^2/Hz, corresponding to a Lorentzian linewidth of 200 kHz [66].
Detection noise	$\delta\phi_{det}$	1 mrad	Allows for imperfect optics, electronics, phase-extraction algorithms.
Gravity gradient coupled with velocity jitter, δv	$k_e\gamma\delta v\ T^3$	0.97 mrad	Assuming differential velocity jitter $\delta v = 0.1$ $\mu m/s$, corresponding to differential lattice frequency difference of 1.5 Hz.
Gravity gradient coupled with position jitter, δr	$k_e\gamma\delta r\ T^2$	0.55 mrad	Assuming differential position jitter $\delta r = 0.3$ μm, to be limited by imperfections of optical transport with 0.39 μm lattice site spacing.
Rotation coupled with velocity jitter, δv	$2k_e\delta v\ c_\Omega\Omega T^2$	0.32 mrad	Assuming suppression of interferometer sensitivity to the orbiting rotation rate Ω by a factor of $c_\Omega = 10^{-3}$ in the cross-track configuration.

for communications with the SE. The GE is likely to include a Mission Operations Center (MOC) operated by the spacecraft provider, and a Science Operations Center (SOC) for end-to-end measurement validation and data processing.

The QGG pathfinder mission will be conducted over the following four defined mission phases: pre-operation (installation through launch); commissioning; calibration & validation ("Operational" Phase); and decommissioning. The pre-operation phase begins with the installation of the instrument. After the instrument is integrated and tested on the spacecraft, the instrument is powered off prior to launch, but the ion pump remains powered on via umbilical power and/or battery power. The spacecraft is then integrated on the launch vehicle, with the spacecraft powered up in launch configuration on the launch pad. The phase ends after successful insertion of the spacecraft at the determined orbit. Once the spacecraft is operationally ready, the power source to the ion pump is switched from battery to on-board power. The potential requirement of an on-board battery powered ion pump is subject to analysis of the maximum vacuum pressure expected prior to in-flight turn on.

The commissioning phase begins with staged power-on basic functionality testing of the QGG subsytems, where the nominal telemetry of health and status from the ICE, the APP, the LOS and the PCU are transmitted to the ground stations via downlink. These tests include individual functional tests of the LOS and the APP to

Table 3 Leading instrument systematic sources and their fractional contributions on gravity gradient measurements. Other effects such as the index of refraction, Gouy phase, differential density shift from beam splitters are determined to be negligible. Note that the sensitivity target of 100mE corresponds to $\approx 83 \times 10^{-6}$ of the nominal gravity gradient. Mean field/density effects have been determined to be below the mrad level [53], with further modelling required to fully quantify it.

Systematic source	**Formula**	**Contribution**	**Comment**
Magnetic field gradient, $\partial_Y B$	$\frac{\hbar}{m}\frac{\alpha}{2}(\partial_Y B)^2 L/(\gamma L)$	2.8×10^{-6}	Second order Zeeman shift $\alpha = \pi \cdot 575$ Hz/G^2 [45]. Assuming constant linear magnetic field gradient, requiring $\partial_Y B < 1.1$ mG/m. While local magnetic force proportional to $B\partial_Y B$, differential magnetic force between two interferometers proportional to $(\partial_Y B)^2 L$.
Wavefront radius of curvature, R	$c_R \frac{\sigma_v^2/R}{\gamma L}$	2.0×10^{-6}	The phase due to wavefront curvature is $k_e \sigma_v^2 T^2/R$ [29, 67], equivalent to an effective acceleration of σ_v^2/R. Assuming the wavefront curvature $R \simeq 1$ km and differing between two interferometers by $c_R \simeq 0.1$.
Misalignment to cross-track, θ_{YY}	$-\theta_{YY}^2$	-1×10^{-6}	Assuming $\lvert\theta_{YY}\rvert < 1$ mrad.
Baseline uncertainty, δL	$\delta L/L$	0.26×10^{-6}	Assuming free-running transport laser frequency uncertainty of 100 MHz, which will be eliminated if offset phase locking by 100 GHz is implemented as described in Section 3.1.2.
Effective wavevector	$\cos\frac{\theta_{AI}}{2} - 1$	-0.13×10^{-6}	Assuming optical frequency error less than 100 kHz, the angle between the counterpropagating Bragg beams $\lvert\theta_{AI}\rvert < 1$ mrad.
Rotation coupled with velocity spread σ_v	$\frac{2k_e \frac{\sigma_v}{\sqrt{N}} c_\Omega \Omega T^2}{k_e \gamma L T^2}$	0.1×10^{-6}	Assuming differential initial velocity can be determined at the level of $\sigma_v/\sqrt{N}$.

verify that the lasers can be locked and sequences can be triggered in the correct order with appropriate timing. After the staged power-on, the instrument is commanded to step through the physics protocol, where diagnostic camera images are used to verify each step. These tests are used to calibrate the instrument in preparation for science-driven campaigns and for technology-driven goals such as to explore parameter space for processes of interest and compare with established models.

The calibration and validation phase is the operational phase of the mission, with the instrument being operated and used to obtain calibration measurements and to perform end-to-end measurement validation campaigns for science and technology. The science-driven campaigns performed during this phase will include forward modeling validation through continuous operation for different time scales: $\sim$ 1 minute

(transient, small amplitude, short-scale features); $\sim$ 10 minutes (local features such as basin-scale hydrology, water resources, small-scale oceanography); $\sim$ 100 minutes (global features such as glacial isostatic adjustment, global mean sea level, land/ocean exchange). Certain pre-defined regions will be revisited multiple times to verify gridded observations through comparison with prior knowledge of the Earth's gravity field, to validate consistency of measurement, and to collect observations over a fixed geographical region. Other planned science-driven campaigns may include continuous operation for longer duration (nominally $\sim$ 30 days for a complete global coverage) for geophysical inversion of largest-scale global features and localized inversion of geophysical features; lower altitude measurements (e.g. gradually transitioning from 400 km to 300 km); and varying the instrument orientation from cross-track to quasi-radial during some science-driven campaigns, to demonstrate the feasibility of a radial QGG. The technology-driven campaigns performed during this phase could include longer interrogation time interferometers, higher Bragg diffraction orders, various atom interferometer configurations, machine-learning optimization, as an opportunity to advance cold atom technology in the unique space microgravity environment and towards SGI.

Knowledge of the spacecraft orbital position and angular orientation are needed to within 1 m and 0.5 mrad, respectively, for measurement validation against Earth's gravity models. A detailed physical model of the spacecraft is needed for the QGG instrument to accurately estimate the spacecraft self-gravity gradient and its thermal and temporal variations to within 100 mE/$\sqrt{Hz}$. While accelerations due to atmospheric drag and other environmental disturbances on the spacecraft are common mode and rejected in QGG measurements, care should be taken on their impact on precise orbital position determination and pointing stability of the spacecraft.

The decommissioning phase will result in the intentional destruction of the spacecraft to comply with NASA policy and standards for orbital debris mitigation.

4.3 Path to a science grade instrument

Pathfinder-QGG requires demonstration of both state-of-the-art techniques and parameters integrated into a single instrument. For Earth observation, as discussed in Section 2.1, orders of magnitude improvements to the sensitivity are required in order to outperform current technologies. There are a few concepts and efforts towards an SGI implementation, such as Refs. [29, 30] among others, exhibiting a large parameter space for critical variables such as the number of measurement axes, altitude, and atomic species. Nevertheless, the consensus is that an SGI QGG should have a sensitivity standard deviation of 10 μE or better. Reaching a science grade instrument, 10,000 times more sensitive than the pathfinder objective, requires beyond state-of-the-art performance in several areas. Both the atom-shot-noise limited sensitivity and the systematic noise sources need to be improved. Equation (3) sheds light on atomic technology development needs.

The baseline L should be extended to the longest feasible for a spacecraft in LEO, say $L = 2$ m for SGI. In addition to SWaP considerations for the platform, establishing the baseline for atom interferometry is a technical challenge. In the physics protocol described in Section 3.2, the baseline of 0.3 m is established via optical lattices. To scale it to meters, parameters such as transport efficiency, accuracy, and heating need

to be reassessed, which may have implications on lattice laser detuning and power requirements. With the knowledge gained through the pathfinder mission and other parallel ground activities, longer transport distances might become an engineering effort rather than a technical challenge. Other approaches exist for lengthening L, such as the concept of two separate atomic sources, transport using magnetic or optical traps, etc.

Achieving 10 $\mu\text{E}/\sqrt{Hz}$ will require significant changes to both interferometer interrogation time as well as orbital orientation. The interrogation time T should be increased to $T = 15$ s. There are no foreseen cold atom technology challenges that prevent achieving long T; however, colder atomic samples would be required to limit the cloud size, placing additional requirements on the laser system, notably increased optical power. Similarly, the sensitivity to rotation and pointing jitter increases as T gets longer. As shown by the simulations in Fig. 1, a radial orbital orientation provides the highest sensitivity to gravity gradients. However, in the radial orientation, the angular velocity of the instrument will be on the order of 1 mrad/s. Uncompensated rotations have been shown to significantly degrade the performance of atom interferometers, both theoretically [29], and experimentally at the lab-scale [65]. A dedicated rotation compensation system within the instrument, and an advanced spacecraft attitude control system might therefore be required to yield meaningful contrast at the highest sensitivity. While the pathfinder is not designed to demonstrate the full sensitivity at longer T, physical models can be validated from various aspect during technology campaigns, e.g., longer T using smaller Bragg order, single interferometer across the two detection regions, etc.

A high-flux, ultra-cold atom source technology is in demand, where $N_d = 10^8$ at pK temperatures is desired. While BEC is the workhorse for generating ultracold ^{87}Rb atoms, paths for generating 10^8 condensed atoms in a SWaP constrained setting are certainly not available today. Moreover, it is desirable to produce ultracold samples at a fast rate, to support interleaved interferometry to be detailed in the following paragraph. Atomic species other than ^{87}Rb may have different cooling technologies toward low temperatures; however, pK is the range of ultimate interest for the SGI, and is not straightforward for any species. It is unrealistic that the pathfinder instrument concept is flexible enough to explore different cooling methods, or different species; nonetheless, its validation of the BEC approach will be a system-level achievement on the capability of implementing complex physics protocol with robustness.

As alluded in Section 2.2 and proposed in literature such as Ref. [29], interleaving atom interferometers is a way to improve sensitivity and sampling rate. Densely interleaved operation, such as 1 Hz sampling rate of $2T = 30$ s interferometers, would improve the sensitivity by a factor of 5. This is a significant technology challenge: these tens of atomic clouds should traverse the same vacuum tube, while being selectively interrogated and detected. The separation of atom source, atom interferometry, and the detection region would be a first step towards interleaving. The pathfinder instrument described above shows some compatibility to interleaving, e.g., capable of shelving atoms in the dark state for near-detuned Bragg pulses; however, a complete demonstrate requires parallel research efforts on the ground.

The size of k_e, i.e., the order of Bragg diffraction, is not a free parameter to drastically increase the sensitivity as suggested in Eq. (3) when the instrument dimension is constrained: For a given T, the larger the k_e, the larger the spatial extent of the interferometer. When two interferometers spatially overlap, the gain in gradient sensitivity starts to diminish. It is optimal to allocate the available space with two adjacent interferometers for QGG, which implies that k_e should be just large enough to move atoms through a given distance in a given time T, which would need $< 100\hbar k$ in most cases. Nevertheless, the QGG pathfinder instrument is capable of implementing interferometers of different k_e, as a validation of physical models and demonstration of physics protocol in a relevant environment.

5 Conclusion

A quantum gravity gradiometer shows promise to be used for low-Earth orbit planetary observation. A successful pathfinder mission outlined in this paper will be the first validation of the QGG measurement concept, and the first end-to-end demonstration of the underlying technology in the relevant operation scenarios. Parallel efforts on technology maturation are required to reach the sensitivity targets of a science-grade QGG. The development of a pathfinder mission payload, funded by NASA Earth Science Technology Office under Earth Science Division, is being implemented by NASA Jet Propulsion Laboratory, Goddard Space Flight Center, and US industry, anticipating delivery and spacecraft integration in 2030.

6 Declarations

6.1 Availability of data and materials

The datasets used and/or analysed during the current study are available from the corresponding author on reasonable request.

6.2 Competing interests

The authors declare that they have no competing interests

6.3 Funding

This work was carried out in part at the Jet Propulsion Laboratory, California Institute of Technology, under a contract with the National Aeronautics and Space Administration. © 2024. All rights reserved. California Institute of Technology. Government sponsorship acknowledged. CSR contributions to the study were funded by NASA grant 80NSSC22K0287. This QGG study was partially funded by the German Federal Ministry for Economic Affairs and Climate Action under DLR contract 50 EE 2312 and 50 EE 2312B.

6.4 Authors' contributions

BS, XB, ML, TS, CO and SC wrote and edited the manuscript. SB, BL and SL established the science motivation and the sensitive curves for the science grade instrument. NL, BM, JH, PG, CK and DW coordinated the development of the pathfinder QGG instrument and mission concept with contributions by all authors. ML, HA, CS and SC developed the concept for the atom interferometer with contributions by NY, RT, HL, PB and AM. TS and AB developed the implementation concept for the laser optical system with contributions by HL, PB, AM, ML and SC. ML, HA, CS and SC developed the error model. XB, CO, PB, AM contributed to the development of the concept of operation.

All authors read and approved the final manuscript.

6.5 Acknowledgements

CSR investigators gratefully acknowledge the use of incomparable supercomputing facilities of the Texas Advanced Computing Center (TACC).

References

[1] Tapley, B.D., Watkins, M.M., Flechtner, F., Reigber, C., Bettadpur, S., Rodell, M., Sasgen, I., Famiglietti, J.S., Landerer, F.W., Chambers, D.P., Reager, J.T., Gardner, A.S., Save, H., Ivins, E.R., Swenson, S.C., Boening, C., Dahle, C., Wiese, D.N., Dobslaw, H., Tamisiea, M.E., Velicogna, I.: Contributions of GRACE to understanding climate change. Nature Climate Change **9**, 358–369 (2019) https://doi.org/10.1038/s41558-019-0456-2

[2] Swenson, S., Wahr, J.: Monitoring the water balance of lake victoria, east africa, from space. Journal of Hydrology **370**(1-4), 163–176 (2009) https://doi.org/10.1016/j.jhydrol.2009.03.008

[3] Voss, K.A., Famiglietti, J.S., Lo, M., De Linage, C., Rodell, M., Swenson, S.C.: Groundwater depletion in the middle east from GRACE with implications for transboundary water management in the tigris-euphrates-western Iran region. Water resources research **49**(2), 904–914 (2013) https://doi.org/10.1002/wrcr.20078

[4] Velicogna, I., Mohajerani, Y., A, G., Landerer, F., Mouginot, J., Noel, B., Rignot, E., Sutterley, T., Broeke, M., Wessem, M., Wiese, D.: Continuity of ice sheet mass loss in greenland and antarctica from the GRACE and GRACE Follow-On missions. Geophysical Research Letters **47** (2020) https://doi.org/10.1029/2020GL087291

[5] Kornfeld, R.P., Arnold, B.W., Gross, M.A., Dahya, N.T., Klipstein, W.M., Gath, P.F., Bettadpur, S.: Grace-fo: The gravity recovery and climate experiment follow-on mission. Journal of Spacecraft and Rockets **56**, 931–951 (2019) https://doi.org/10.2514/1.A34326

[6] Li, B., Rodell, M., Kumar, S., Beaudoing, H.K., Getirana, A., Zaitchik, B.F., Goncalves, L.G., Cossetin, C., Bhanja, S., Mukherjee, A., Tian, S., Tangdamrongsub, N., Long, D., Nanteza, J., Lee, J., Policelli, F., Goni, I.B., Daira, D., Bila, M., Lannoy, G., Mocko, D., Steele-Dunne, S.C., Save, H., Bettadpur, S.: Global GRACE data assimilation for groundwater and drought monitoring: Advances and challenges. Water Resources Research **55**, 7564–7586 (2019) https://doi.org/10.1029/2018WR024618

[7] Sciences, N.A., Engineering, D., Sciences, P., Board, S.S., Earth Science, C., Space, A.: Thriving on Our Changing Planet: A Decadal Strategy for Earth Observation from Space. National Academies Press, ??? (2019)

[8] Overstreet, C., Asenbaum, P., Curti, J., Kim, M., Kasevich, M.A.: Observation of a gravitational Aharonov-Bohm effect. Science **375**, 226–229 (2022) https://doi.org/10.1126/science.abl7152

[9] Niebauer, T.M., Billson, R., Ellis, B., Mason, B., Westrum, D., Klopping, F.: Simultaneous gravity and gradient measurements from a recoil-compensated absolute gravimeter. Metrologia **48**, 154–163 (2011) https://doi.org/10.1088/0026-1394/48/3/009

[10] Vovrosh, J., Dragomir, A., Stray, B., Boddice, D.: Advances in portable atom interferometry-based gravity sensing. Sensors **23**, 7651 (2023) https://doi.org/10.3390/s23177651

[11] Kasevich, M., Chu, S.: Atomic interferometry using stimulated Raman transitions. Physical Review Letters **67**, 181–184 (1991) https://doi.org/10.1103/PhysRevLett.67.181

[12] Snadden, M., McGuirk, J., Bouyer, P., Haritos, K., Kasevich, M.: Measurement of the Earth's gravity gradient with an atom interferometer-based gravity gradiometer. Physical Review Letters **81**, 971–974 (1998) https://doi.org/10.1103/PhysRevLett.81.971

[13] Stray, B., Lamb, A., Kaushik, A., Vovrosh, J., Rodgers, A., Winch, J., Hayati, F., Boddice, D., Stabrawa, A., Niggebaum, A., Langlois, M., Lien, Y.-H., Lellouch, S., Roshanmanesh, S., Ridley, K., Villiers, G., Brown, G., Cross, T., Tuckwell, G., Faramarzi, A., Metje, N., Bongs, K., Holynski, M.: Quantum sensing for gravity cartography. Nature **602**, 590–594 (2022) https://doi.org/10.1038/s41586-021-04315-3

[14] Antoni-Micollier, L., Carbone, D., Ménoret, V., Lautier-Gaud, J., King, T., Greco, F., Messina, A., Contrafatto, D., Desruelle, B.: Detecting volcano-related underground mass changes with a quantum gravimeter. Geophysical Research Letters **49** (2022) https://doi.org/10.1029/2022GL097814

[15] Müntinga, H., Ahlers, H., Krutzik, M., Wenzlawski, A., Arnold, S., Becker, D.,

Bongs, K., Dittus, H., Duncker, H., Gaaloul, N., *et al.*: Interferometry with bose-einstein condensates in microgravity. Physical review letters **110**(9), 093602 (2013) https://doi.org/10.1103/PhysRevLett.110.093602

[16] Deppner, C., Herr, W., Cornelius, M., Stromberger, P., Sternke, T., Grzeschik, C., Grote, A., Rudolph, J., Herrmann, S., Krutzik, M., Wenzlawski, A., Corgier, R., Charron, E., Guéry-Odelin, D., Gaaloul, N., Lämmerzahl, C., Peters, A., Windpassinger, P., Rasel, E.M.: Collective-mode enhanced matter-wave optics. Phys. Rev. Lett. **127**, 100401 (2021) https://doi.org/10.1103/PhysRevLett.127.100401

[17] Pelluet, C., Arguel, R., Rabault, M., Jarlaud, V., Metayer, C., Barrett, B., Bouyer, P., Battelier, B.: Atom interferometry in an Einstein Elevator (2024). https://arxiv.org/abs/2407.07183

[18] Condon, G., Rabault, M., Barrett, B., Chichet, L., Arguel, R., Eneriz-Imaz, H., Naik, D., Bertoldi, A., Battelier, B., Bouyer, P., Landragin, A.: All-optical bose-einstein condensates in microgravity. Physical Review Letters **123**, 240402 (2019) https://doi.org/10.1103/PhysRevLett.123.240402

[19] Vogt, C., Woltmann, M., Herrmann, S., Lämmerzahl, C., Albers, H., Schlippert, D., Rasel, E.M.: Evaporative cooling from an optical dipole trap in microgravity. Physical Review A **101**, 013634 (2020) https://doi.org/10.1103/PhysRevA.101.013634

[20] Barrett, B., Antoni-Micollier, L., Chichet, L., Battelier, B., Lévèque, T., Landragin, A., Bouyer, P.: Dual matter-wave inertial sensors in weightlessness. Nature Communications **7**, 13786 (2016) https://doi.org/10.1038/ncomms13786

[21] Becker, D., Lachmann, M.D., Seidel, S.T., Ahlers, H., Dinkelaker, A.N., Grosse, J., Hellmig, O., Müntinga, H., Schkolnik, V., Wendrich, T., Wenzlawski, A., Weps, B., Corgier, R., Franz, T., Gaaloul, N., Herr, W., Lüdtke, D., Popp, M., Amri, S., Duncker, H., Erbe, M., Kohfeldt, A., Kubelka-Lange, A., Braxmaier, C., Charron, E., Ertmer, W., Krutzik, M., Lämmerzahl, C., Peters, A., Schleich, W.P., Sengstock, K., Walser, R., Wicht, A., Windpassinger, P., Rasel, E.M.: Space-borne Bose–Einstein condensation for precision interferometry. Nature **562**, 391–395 (2018) https://doi.org/10.1038/s41586-018-0605-1

[22] Elliott, E.R., Krutzik, M.C., Williams, J.R., Thompson, R.J., Aveline, D.C.: NASA's Cold Atom Lab (CAL): system development and ground test status. npj Microgravity **4**, 16 (2018) https://doi.org/10.1038/s41526-018-0049-9

[23] Elliott, E.R., Aveline, D.C., Bigelow, N.P., Boegel, P., Botsi, S., Charron, E., D'Incao, J.P., Engels, P., Estrampes, T., Gaaloul, N., Kellogg, J.R., Kohel, J.M., Lay, N.E., Lundblad, N., Meister, M., Mossman, M.E., Müller, G., Müller, H., Oudrhiri, K., Phillips, L.E., Pichery, A., Rasel, E.M., Sackett, C.A., Sbroscia, M., Schleich, W.P., Thompson, R.J., Williams, J.R.: Quantum gas mixtures and

dual-species atom interferometry in space. Nature **623**, 502–508 (2023) https://doi.org/10.1038/s41586-023-06645-w

[24] Core Writing Team, H.L., (eds.), J.R.: Sections. in: Climate change 2023: Synthesis report. contribution of working groups i, ii and iii to the sixth assessment report of the intergovernmental panel on climate change. IPCC, 35–115 (2023) https://doi.org/10.59327/IPCC/AR6-9789291691647

[25] National Academies of Sciences, Engineering, and Medicine: Thriving on Our Changing Planet: A Decadal Strategy for Earth Observation from Space. The National Academies Press, Washington, DC (2018). https://doi.org/10.17226/24938 . https://nap.nationalacademies.org/catalog/24938/thriving-on-our-changing-planet-a-decadal-strategy-for-earth

[26] Wiese, D.N., Bienstock, B., Blackwood, C., Chrone, J., Loomis, B.D., Sauber, J., Rodell, M., Baize, R., Bearden, D., Case, K., Horner, S., Luthcke, S., Reager, J.T., Srinivasan, M., Tsaoussi, L., Webb, F., Whitehurst, A., Zlotnicki, V.: The mass change designated observable study: Overview and results. Earth and Space Science **9**(8) (2022) https://doi.org/10.1029/2022ea002311

[27] Luthcke, S.B., Saif, B., Fisher, K., Baird, L.R., Loomis, B., Everett, D., Banting, R., Piepmeier, J., Shappirio, M., Rowlands, D.: Atom interferometer gravity gradiometer (AIGG) instrument technology development readiness, flight implementation, and expected performance, v 3.1_nec. Technical report, NASA Goddard Space Flight Center, AOSense (June 2021). https://smd-cms.nasa.gov/wp-content/uploads/2023/05/1AIGGInstrumentTechnologyDevelopmentReadinessFlightImplementationandExpectedPerformance.pdf

[28] Yu, N., Chiow, S.-w., Bettadpur, S.: Mass change hybrid SST-QGG technology report. Technical report, JPL (2023). https://smd-cms.nasa.gov/wp-content/uploads/2023/05/2MCHybridSST_QGGTechnologyReport.pdf

[29] Trimeche, A., Battelier, B., Becker, D., Bertoldi, A., Bouyer, P., Braxmaier, C., Charron, E., Corgier, R., Cornelius, M., Douch, K., Gaaloul, N., Herrmann, S., Müller, J., Rasel, E., Schubert, C., Wu, H., Santos, F.: Concept study and preliminary design of a cold atom interferometer for space gravity gradiometry. Classical and Quantum Gravity **36**(21) (2019) https://doi.org/10.1088/1361-6382/ab4548

[30] Carraz, O., Siemes, C., Massotti, L., Haagmans, R., Silvestrin, P.: A spaceborne gravity gradiometer concept based on cold atom interferometers for measuring Earth's gravity field. Microgravity Science and Technology **26**(3), 139–145 (2014) https://doi.org/10.1007/s12217-014-9385-x

[31] Rudolph, J., Gaaloul, N., Singh, Y., Ahlers, H., Herr, W., Schulze, T.A., Seidel, S.T., Rode, C., Schkolnik, V., Ertmer, W., Rasel, E.M., Müntinga, H., Könemann, T., Resch, A., Herrmann, S., Lämmerzahl, C., Zoest, T., Dittus, H., Vogel, A.,

Wenzlawski, A., Sengstock, K., Meyer, N., Bongs, K., Krutzik, M., Lewoczko-Adamczyk, W., Schiemangk, M., Peters, A., Eckart, M., Kajari, E., Arnold, S., Nandi, G., Schleich, W.P., Walser, R., Steinmetz, T., Hänsch, T.W., Reichel, J.: Degenerate quantum gases in microgravity. Microgravity Science and Technology **23**, 287–292 (2011) https://doi.org/10.1007/s12217-010-9247-0

[32] Lachmann, M.D., Ahlers, H., Becker, D., Dinkelaker, A.N., Grosse, J., Hellmig, O., Müntinga, H., Schkolnik, V., Seidel, S.T., Wendrich, T., Wenzlawski, A., Carrick, B., Gaaloul, N., Lüdtke, D., Braxmaier, C., Ertmer, W., Krutzik, M., Lämmerzahl, C., Peters, A., Schleich, W.P., Sengstock, K., Wicht, A., Windpassinger, P., Rasel, E.M.: Ultracold atom interferometry in space. Nature Communications **12**(1), 1317 (2021) https://doi.org/10.1038/s41467-021-21628-z

[33] Williams, J.R., Sackett, C.A., Ahlers, H., Aveline, D.C., Boegel, P., Botsi, S., Charron, E., Elliott, E.R., Gaaloul, N., Giese, E., Herr, W., Kellogg, J.R., Kohel, J.M., Lay, N.E., Meister, M., Müller, G., Müller, H., Oudrhiri, K., Phillips, L., Pichery, A., Rasel, E.M., Roura, A., Sbroscia, M., Schleich, W.P., Schneider, C., Schubert, C., Sen, B., Thompson, R.J., Bigelow, N.P.: Pathfinder experiments with atom interferometry in the cold atom lab onboard the international space station. Nature Communications **15**, 6414 (2024) https://doi.org/10.1038/s41467-024-50585-6

[34] Kovachy, T., Asenbaum, P., Overstreet, C., Donnelly, C.A., Dickerson, S.M., Sugarbaker, A., Hogan, J.M., Kasevich, M.A.: Quantum superposition at the half-metre scale. Nature 2015 528:7583 **528**, 530–533 (2015) https://doi.org/10.1038/nature16155

[35] Parker, R.H., Yu, C., Estey, B., Zhong, W., Huang, E., Müller, H.: Controlling the multiport nature of Bragg diffraction in atom interferometry. Physical Review A **94**, 053618 (2016) https://doi.org/10.1103/PHYSREVA.94.053618/FIGURES/13/MEDIUM

[36] Kirsten-Siemß, J.-N., Fitzek, F., Schubert, C., Rasel, E.M., Gaaloul, N., Hammerer, K.: Large-momentum-transfer atom interferometers with μ rad-accuracy using bragg diffraction. Physical Review Letters **131**, 033602 (2023) https://doi.org/10.1103/PhysRevLett.131.033602

[37] Cheinet, P., Canuel, B., Pereira Dos Santos, F., Gauguet, A., Yver-Leduc, F., Landragin, A.: Measurement of the sensitivity function in a time-domain atomic interferometer. IEEE Transactions on Instrumentation and Measurement **57**(6), 1141–1148 (2008) https://doi.org/10.1109/TIM.2007.915148

[38] Kovachy, T., Hogan, J.M., Sugarbaker, A., Dickerson, S.M., Donnelly, C.A., Overstreet, C., Kasevich, M.A.: Matter wave lensing to picokelvin temperatures. Physical Review Letters **114**, 143004 (2015) https://doi.org/10.1103/PhysRevLett.114.143004

[39] Gaaloul, N., Meister, M., Corgier, R., Pichery, A., Boegel, P., Herr, W., Ahlers, H., Charron, E., Williams, J.R., Thompson, R.J., Schleich, W.P., Rasel, E.M., Bigelow, N.P.: A space-based quantum gas laboratory at picokelvin energy scales. Nature Communications **13**(1) (2022) https://doi.org/10.1038/s41467-022-35274-6

[40] Burke, J.P., Bohn, J.L., Esry, B.D., Greene, C.H.: Prospects for mixed-isotope Bose-Einstein condensates in rubidium. Physical Review Letters **80**, 2097–2100 (1998) https://doi.org/10.1103/PhysRevLett.80.2097

[41] Jenkins, D.R.: The determination of cross sections for the quenching of resonance radiation of metal atoms ii. results for potassium, rubidium and caesium. Proceedings of the Royal Society of London. Series A. Mathematical and Physical Sciences **303**, 453–465 (1968) https://doi.org/10.1098/rspa.1968.0060

[42] Frye, K., Abend, S., Bartosch, W., Bawamia, A., Becker, D., Blume, H., Braxmaier, C., Chiow, S.-W., Efremov, M.A., Ertmer, W., Fierlinger, P., Franz, T., Gaaloul, N., Grosse, J., Grzeschik, C., Hellmig, O., Henderson, V.A., Herr, W., Israelsson, U., Kohel, J., Krutzik, M., Kürbis, C., Lämmerzahl, C., List, M., Lüdtke, D., Lundblad, N., Marburger, J.P., Meister, M., Mihm, M., Müller, H., Müntinga, H., Nepal, A.M., Oberschulte, T., Papakonstantinou, A., Perovsěk, J., Peters, A., Prat, A., Rasel, E.M., Roura, A., Sbroscia, M., Schleich, W.P., Schubert, C., Seidel, S.T., Sommer, J., Spindeldreier, C., Stamper-Kurn, D., Stuhl, B.K., Warner, M., Wendrich, T., Wenzlawski, A., Wicht, A., Windpassinger, P., Yu, N., Wörner, L.: The Bose-Einstein condensate and cold atom laboratory. EPJ Quantum Technology **8**, 1 (2021) https://doi.org/10.1140/epjqt/s40507-020-00090-8

[43] Papoyan, A., Shmavonyan, S., Khanbekyan, A., -, Jaatinen, E., Hopper, D.J., -, J.B., McCarron, D.J., King, S.A., Cornish, S.L.: Modulation transfer spectroscopy in atomic rubidium. Measurement Science and Technology **19**, 105601 (2008) https://doi.org/10.1088/0957-0233/19/10/105601

[44] Zhou, O., Neely, A.O., Pagel, Z.R., Bernstein, M., Roth, J., Mueller, H.: Offset lock with a 440-Ghz range using electro-optic modulation. Optics Continuum **2**, 1087 (2023) https://doi.org/10.1364/optcon.474038

[45] Steck, D.A.: Rubidium 87 D line data (2001). http://steck.us/alkalidata

[46] McGuirk, J.M.: Sensitive absolute-gravity gradiometry using atom interferometry. Physical Review A **65**(3) (2002) https://doi.org/10.1103/PhysRevA.65.033608

[47] Chiow, S.-w., Williams, J., Yu, N.: Noise reduction in differential phase extraction of dual atom interferometers using an active servo loop. Physical Review A **93**(1) (2016) https://doi.org/10.1103/PhysRevA.93.013602

[48] Petrich, W., Anderson, M.H., Ensher, J.R., Cornell, E.A.: Stable, tightly confining

magnetic trap for evaporative cooling of neutral atoms. Physical Review Letters **74**, 3352–3355 (1995) https://doi.org/10.1103/PhysRevLett.74.3352

[49] Camparo, J.C., Frueholz, R.P.: A dressed atom interpretation of adiabatic rapid passage. Journal of Physics B: Atomic and Molecular Physics **17**, 4169–4178 (1984) https://doi.org/10.1088/0022-3700/17/20/015

[50] Peik, E., Dahan, M.B., Bouchoule, I., Castin, Y., Salomon, C.: Bloch oscillations of atoms, adiabatic rapid passage, and monokinetic atomic beams. Physical Review A **55**, 2989–3001 (1997) https://doi.org/10.1103/PhysRevA.55.2989

[51] Gebbe, M., Siemß, J.-N., Gersemann, M., Müntinga, H., Herrmann, S., Lämmerzahl, C., Ahlers, H., Gaaloul, N., Schubert, C., Hammerer, K., Abend, S., Rasel, E.M.: Twin-lattice atom interferometry. Nature Communications **12**, 2544 (2021) https://doi.org/10.1038/s41467-021-22823-8

[52] Pagel, Z., Zhong, W., Parker, R.H., Olund, C.T., Yao, N.Y., Müller, H.: Symmetric bloch oscillations of matter waves. Physical Review A **102**, 053312 (2020) https://doi.org/10.1103/PhysRevA.102.053312

[53] Williams, J., Chiow, S.-w., Yu, N., Müller, H.: Quantum test of the equivalence principle and space-time aboard the international space station. New Journal of Physics **18**(2), 025018 (2016) https://doi.org/10.1088/1367-2630/18/2/025018

[54] Chiow, S.-w., Kovachy, T., Chien, H.-C., Kasevich, M.A.: 102 $\hbar k$ large area atom interferometers. Physical review letters **107**(13), 130403 (2011) https://doi.org/10.1103/PhysRevLett.107.130403

[55] Berg, P., Abend, S., Tackmann, G., Schubert, C., Giese, E., Schleich, W.P., Narducci, F.A., Ertmer, W., Rasel, E.M.: Composite-light-pulse technique for high-precision atom interferometry. Physical Review Letters **114**, 063002 (2015) https://doi.org/10.1103/PhysRevLett.114.063002

[56] Louie, G., Chen, Z., Deshpande, T., Kovachy, T.: Robust atom optics for Bragg atom interferometry. New Journal of Physics **25**, 083017 (2023) https://doi.org/10.1088/1367-2630/aceb15

[57] Dickerson, S.M., Hogan, J.M., Sugarbaker, A., Johnson, D.M.S., Kasevich, M.A.: Multiaxis inertial sensing with long-time point source atom interferometry. Phys. Rev. Lett. **111**, 083001 (2013) https://doi.org/10.1103/PhysRevLett.111.083001

[58] Sugarbaker, A., Dickerson, S.M., Hogan, J.M., Johnson, D.M.S., Kasevich, M.A.: Enhanced atom interferometer readout through the application of phase shear. Phys. Rev. Lett. **111**, 113002 (2013) https://doi.org/10.1103/PhysRevLett.111.113002

[59] Overstreet, C., Asenbaum, P., Kovachy, T., Notermans, R., Hogan, J.M., Kasevich, M.A.: Effective inertial frame in an atom interferometric test of the equivalence principle. Physical Review Letters **120**(18) (2018) https://doi.org/10.1103/PhysRevLett.120.183604

[60] Wigley, P.B., Hardman, K.S., Freier, C., Everitt, P.J., Legge, S., Manju, P., Close, J.D., Robins, N.P.: Readout-delay-free Bragg atom interferometry using overlapped spatial fringes. Physical Review A **99**(2) (2019) https://doi.org/10.1103/PhysRevA.99.023615

[61] Ben-Aïcha, Y., Mehdi, Z., Freier, C., Szigeti, S.S., Wigley, P.B., Conlon, L.O., Husband, R., Legge, S., Eagle, R.H., Hope, J.J., Robins, N.P., Close, J.D., Hardman, K.S., Haine, S.A., Thomas, R.J.: A Dual Open Atom Interferometer for Compact, Mobile Quantum Sensing. arXiv:2405.00400 (2024). https://ui.adsabs.harvard.edu/abs/2024arXiv240500400B

[62] Tackmann, G., Berg, P., Schubert, C., Abend, S., Gilowski, M., Ertmer, W., Rasel, E.M.: Self-alignment of a compact large-area atomic sagnac interferometer. New Journal of Physics **14**(1), 015002 (2012) https://doi.org/10.1088/1367-2630/14/1/015002

[63] Roura, A.: Circumventing heisenberg's uncertainty principle in atom interferometry tests of the equivalence principle. Physical Review Letters **118**(16) (2017) https://doi.org/10.1103/PhysRevLett.118.160401

[64] Kleinert, S., Kajari, E., Roura, A., Schleich, W.P.: Representation-free description of light-pulse atom interferometry including non-inertial effects. Physics Reports **605**, 1–50 (2015) https://doi.org/10.1016/j.physrep.2015.09.004

[65] Lan, S.-Y., Kuan, P.-C., Estey, B., Haslinger, P., Müller, H.: Influence of the coriolis force in atom interferometry. Phys. Rev. Lett. **108**, 090402 (2012) https://doi.org/10.1103/PhysRevLett.108.090402

[66] Le Gouët, J., Cheinet, P., Kim, J., Holleville, D., Clairon, A., Landragin, A., Pereira Dos Santos, F.: Influence of lasers propagation delay on the sensitivity of atom interferometers. The European Physical Journal D **44**(3), 419–425 (2007) https://doi.org/10.1140/epjd/e2007-00218-2

[67] Louchet-Chauvet, A., Farah, T., Bodart, Q., Clairon, A., Landragin, A., Merlet, S., Santos, F.P.D.: The influence of transverse motion within an atomic gravimeter. New Journal of Physics **13**(6), 065025 (2011) https://doi.org/10.1088/1367-2630/13/6/065025